



## **Final Draft** **of the original manuscript**

Jin, F.; Rao, H.; Wang, Q.; Wen, G.; Liu, P.; Liu, J.; Shen, J.; Li, J.;  
Xiong, J.; Ma, N.:

**Heat-pattern induced non-uniform radial microstructure and  
properties of Ti-6Al-4V joint prepared by rotary friction  
welding**

In: Materials Characterization. Vol. 195 (2023) 112536.

First published online by Elsevier: 29.11.2022

<https://dx.doi.org/10.1016/j.matchar.2022.112536>

**Heat-pattern induced non-uniform radial microstructure and properties of Ti-6Al-4V joint prepared by rotary friction welding**

Feng Jin<sup>a,b</sup>, Haodong Rao<sup>a</sup>, Qian Wang<sup>c,\*</sup>, Guodong Wen<sup>d</sup>, Pu Liu<sup>a</sup>,  
Jiatao Liu<sup>a</sup>, Junjun Shen<sup>b</sup>, Jinglong Li<sup>a</sup>, Jiangtao Xiong<sup>a</sup>, Ninshu Ma<sup>c</sup>

<sup>a</sup> Shaanxi Key Laboratory of Friction Welding Technologies, Northwestern Polytechnical

University, Xi'an 710072, PR China

<sup>b</sup> Helmholtz-Zentrum Hereon, Institute of Materials Mechanics, Solid State Materials

Processing, Max-Planck-Str. 1, Geesthacht 21502, Germany

<sup>c</sup> Joining and Welding Research Institute, Osaka University, Osaka 567-0047, Japan

<sup>d</sup> Xi'an Research Institute of China Coal Technology & Engineering Group Corp, Xi'an,

710077, People's Republic of China

Corresponding author: Qian Wang

E-mail: [qianwang@jwri.osaka-u.ac.jp](mailto:qianwang@jwri.osaka-u.ac.jp)

## **Abstract**

Heat-pattern (HP) induced non-uniform radial microstructure and properties of rotary friction welded Ti-6Al-4V joint was focused in this study, the formation mechanism of which was clarified by  $\beta$ -reconstruction. The results show that Ti-6Al-4V friction welded heat-pattern at different rotational speeds can be generally separated into ‘glass-like’ HP and ‘scissor-like’ HP. According to the results of  $\beta$ -reconstruction, the radial microstructures of ‘glass-like’ HP and ‘scissor-like’ HP are deformed  $\alpha$  grains  $\rightarrow$  deformed  $\alpha$  grains and lamellar  $\alpha'$  laths  $\rightarrow$  lamellar  $\alpha'$  laths corresponding to center  $\rightarrow$  1/2R  $\rightarrow$  periphery respectively, where lamellar  $\alpha'$  laths at periphery of ‘scissor-like’ HP have similar orientations to form  $\alpha'$  colony. Deformed  $\alpha$  grains at center zone make the strength higher than that of base metal (BM) and share the similar morphology of BM compared with the lamellar  $\alpha'$  laths, to get the highest elongation among the three regions of center, 1/2R and periphery, reaching near 80% of BM. Whereas, lamellar  $\alpha'$  laths at periphery share a coarser size than that of the center zone, the strength of which is reduced and close to the BM. Compared with the deformed  $\alpha$  grains, lamellar  $\alpha'$  laths are quite different from BM in morphology, which causes a significant reduction in elongation to only 62.1% of BM. Aggravating the issue further, the elongation of ‘scissor - like’ HP is reduced to only 50.3% of BM at periphery because of  $\alpha'$  colony. Therefore, the strength and elongation of the joint decrease gradually from center to periphery.

**Keywords: Titanium, Rotary friction welding, Heat-pattern, Radial microstructure,  $\beta$ -reconstruction**

## 1. Introduction

Titanium alloys are widely employed in airplane structural components because of their high strength, low density, and outstanding fatigue qualities [1-3]. When joining titanium alloys with diverse structures or compositions, friction welding and electron beam welding are the two common methods for producing high-quality joints [4,5]. Rotary friction welding (RFW), the most popular variation of friction welding technologies, is the best solution for combining rotating components in the aerospace industry, such as shaft-disk assemblies [6-8]. However, the radial microstructure and characteristics of a rotary friction welded joint have been reported to be non-uniformly distributed over the welded interface [9-10], posing a challenge to the aeronautical structural joint's reliability and necessitating more systematic researches.

RFW creates a joint heat-pattern (HP) to accomplish solid-state bonding at the initial contact [8,10-13]. Fig.1 depicts the variations of reported heat-patterns under various rotational speeds and pressures [8,10,12,13], where Fig.1a shows heat patterns of steel summarized from experimental studies [8,12] and Fig.1b the heat-patterns of AA6061. In fact, rotational speed is widely utilized to control HP in industry because welding pressure is less effective when it exceeds 40MPa [10,13], as demonstrated in Fig.1b, which uses rotational speed to control HP of the readily deformed AA6061. HP plays a dominating role in joint formation during RFW at various rotational speeds. Therefore, in recent decades, experimental and computational investigations have been conducted in an attempt to elucidate the formation mechanism of heat-patterns with rotational speeds [7,14-16]. And it has been clarified that HP is actually the morphology

of plasticized metal at the interface [8,17,18]. Kimura [14], Li [15], and Jin [16] then used the initiation and evolution of plasticized metal at varied rotational speeds to differentiate the heat-patterns experimentally. Jin [7] further simulated this process based on the friction coefficients gathered throughout the friction process in order to elucidate the development of an HP. However, the preceding literatures focused on the rotary friction welded HP of steel [8,12] and aluminum alloys [10,13], and few attempts have been made to research and assess the HP of titanium alloys.

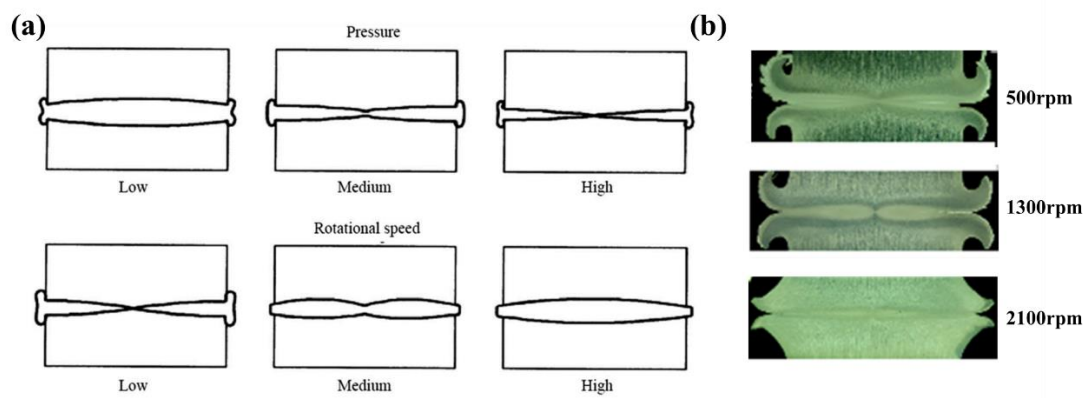


Fig.1 Variations of reported heat-pattern under different welding conditions:

(a) heat patterns of steel summarized from experimental studies [8,12] and (b) heat-patterns of AA6061 at different rotational speeds under a pressure of 40MPa [10,13]

Heat-pattern has been proved to be the morphology of plasticized metal formed at the interface. Hence, distinct heat-patterns suggest varied radial microstructures along the welded line, which becomes more complicated when friction-fabricating titanium alloys with phase transition. Therefore, detailed descriptions of the microstructure are often given without identifying the original bonds between the interfaces [19,20] and the formation of the varied microstructures of titanium friction welded joint is explained graphically according to hypothesis [21,22]. As an example, Wang [21] gave a detailed

description of the microstructure (equiaxed  $\alpha$  grains, lamellar  $\alpha'$  laths) and thoroughly characterized the microtexture of a linear friction welded Ti-6.5Al-3.5Mo-1.5Zr-0.3Si joint. Kim [22] graphically explained the formation of varied microstructures at different zones of a friction stir welded Ti-6Al-4V joint. However, they didn't clarify the interfacial mechanisms responsible for solid-state bonding so that the underlying mechanisms leading to the varied radial microstructures of a titanium (alloys with phase transition) friction welded joint. Accounting for this, the microstructure during welding process cannot be observed and the microstructure of the joint has undergone a phase transition. That means, ' $\beta$  grains' at welding temperature can influence the dominant formation mechanism of microstructures of the titanium joint, which however cannot be easily characterized directly at room temperature. In the last decade, the Electron Back-Scattered Diffraction (EBSD) technique has been employed to study  $\beta$ - $\alpha$  phase transformation by in-situ experiment [23,24] and the ' $\beta$ -reconstruction' technology was developed by Humbert et al. [25-27], where the  $\beta$  grains were reconstructed according to inherent  $\alpha$  orientations (Burgers relationship). In fact, there are only a limited number of misorientations across  $\alpha$  variants that derive from the same  $\beta$  grain [28]. Triple junctions of  $\alpha$  grains that have misorientations compatible with a common  $\beta$  orientations are identified first and used to compute the  $\beta$  orientation. This technology now has been used to explore the morphology of high-temperature  $\beta$  grains in titanium [29] and attempted to identify  $\beta$  grains at welding temperature. As an example, Xavier [30] successfully reconstructed  $\beta$  grains of Ti6242/Ti17 linear friction welded joint during welding process in 2019. However, the technic hasn't been used to clarify the

formation mechanism of radial microstructures (i.e., equiaxed  $\alpha$  grains, lamellar  $\alpha'$  laths) of Ti-6Al-4V joint.

Heat-pattern induced non-uniform radial microstructure will cause the inhomogeneous mechanical properties along the welded line. Li [10] reported the non-uniform microstructures and properties of AA6061 rotary friction welded joint. Wang [21] was the first to notice inhomogeneous microstructures and their impact on the joint mechanical properties of a Ti-6.5Al-3.5Mo-1.5Zr-0.3Si linear friction welded joint. Li [31] comprehensively investigated the heat-pattern induced inhomogeneous radial microstructure and mechanical properties of rotary friction welded AA2024 joints. The above researches demonstrated the significance of studying heat-pattern induced non-uniform radial microstructure and mechanical properties in friction welding. However, non-uniform radial microstructures and their impact on the mechanical properties of a titanium alloy rotary friction welded joint were rarely discussed.

The work presented here addresses these complicated issues based on novel experimental studies coupled with simulation analyses.  $\beta$ -reconstruction was at first time employed to clarify the formation of non-uniform microstructures so that the non-uniform properties of a friction welded joint. Ti-6Al-4V was selected as the base metal (BM) for its wide range of applications in aviation. RFW experiments were carried out at various rotational speeds to acquire varied heat-patterns, where the friction torque and temperature were captured for data preparation used in simulation. The formation mechanism of different Ti-6Al-4V heat-patterns were clarified by the simulation results. Inner different heat-patterns, the varied radial microstructures were characterized by

EBSD to offer the data for  $\beta$ -reconstruction to understand the underlying mechanisms leading to the varied radial microstructures of a titanium friction welded joint. At last, the effects of non-uniform radial microstructures of different heat-patterns on the mechanical properties were analyzed.

## **2. Experimental**

Rods of commercially available Ti-6Al-4V in diameter of  $\phi 25\text{mm}$  were used as base metals, whose chemical composition is listed in Table 1. Fig.2 shows the microstructure of the base metal characterized by inverse pole figure (IPF) map and phase distribution with grain boundary, which is mainly consisted of equiaxed  $\alpha$  grains. Before welding, the faying surfaces of the specimens were polished to eliminate the effect of surface roughness and ultrasonically cleaned in alcohol and dried in air. To investigate different heat-patterns of Ti-6Al-4V joint welded varied with rotational speeds, RFW experiments were conducted on a continuous-drive rotary friction welding machine (C320, Hanzhong Shuangji Friction Welding Techniques Co. Ltd., China). Rotational speeds were designed for a wide range of 500rpm to 1800rpm (i.e., 500, 900, 1200, 1500, 1800rpm), where the welding pressure was set as 40MPa and burn-off length 5mm. Fig.3 shows the detailed dimensions of specimens and layout for RFW experiments. During the welding process, friction torque, surface temperature and burn-off rate were captured for data preparations used in simulation. Temperature was sampled using an infrared thermographic camera (InfraTec VarioCAM® hr head-HS) at a frame rate of 50 fps and the burn-off rate was measured using a high-speed camera (Phantom V310, Vision Research. Inc).

Table 1 Nominal chemical composition of Ti-6Al-4V titanium alloy (wt.%)

Ti	Al	V	Fe	O	C	N	H
Bal.	6.1	4.1	0.28	0.18	0.08	0.03	0.01

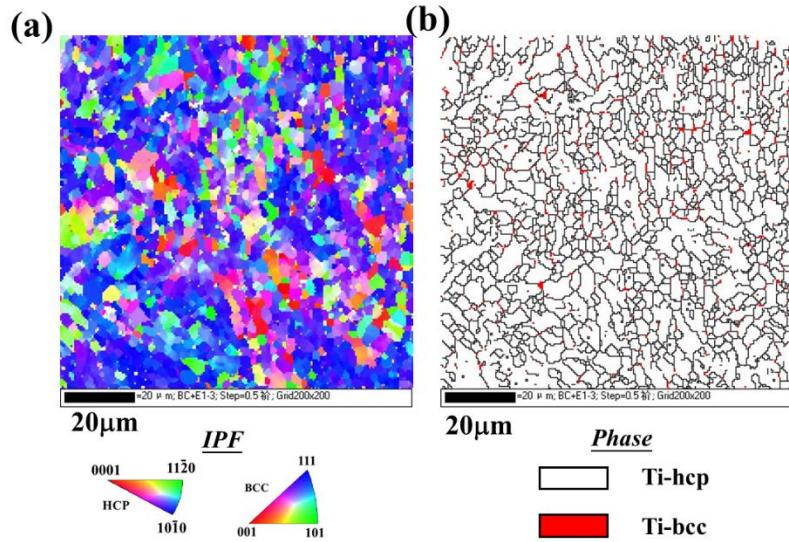


Fig.2 Microstructure of Ti-6Al-4V base metal characterized by (a) IPF map and (b) phase distribution with grain boundary

After welding, cross-sections were then cut from the joints for optical and EBSD examination. To show the morphologies of heat-patterns, the sections were mounted, ground, polished and etched by a solution ( $\text{HNO}_3$ :  $\text{HF}$ :  $\text{H}_2\text{O}$  = 1:2:17 in volume). The morphology examinations were performed by an optical microscope (OM, OLYMPUS PMG3) and the rough microstructure examinations by a scanning electron microscope (SEM, ZEISS Gemini 500). To further differ the radial microstructures inner heat-patterns and prepare the microstructural data for  $\beta$ -reconstruction to clarify the mechanisms leading to the varied radial microstructures, EBSD was employed to characterize five featured zones along the welded line, shown in Fig.3b. The mechanical polished sections were then electro-polished in a solution ( $\text{HClO}_4$ :  $\text{C}_4\text{H}_9\text{OH}$ :  $\text{CH}_3\text{OH}$  =

3:15:32 in volume). EBSD observations were carried out parallel to the rolling axis using the OXFORD NORDLYS X-MAX system and HKL-Channel5 software. Fig.3b shows the employed reference frame that will be used in microstructure analysis. The step size for the EBSD scan was  $0.35\mu\text{m}$ . After getting the EBSD data,  $\beta$ -reconstruction was conducted according to Bachmann's work [24-25] to reveal the mechanisms leading to the varied radial microstructure. The recrystallized distribution map was employed to analyze the recrystallized behaviors of the grains, where blue grains represent recrystallized grains, yellow grains represent sub-grains and red grains represent deformed grains

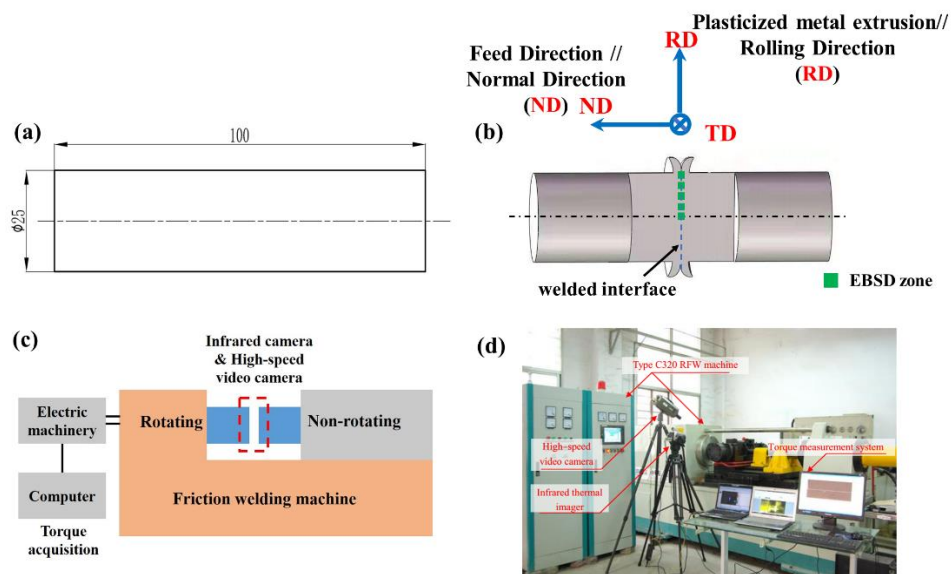


Fig.3 Rod-structure specimen and layout for RFW experiments showing

(a) the detailed dimensions, (b) the employed reference frame,

(c) the system composition and (d) the experimental setup

To investigate the effects of non-uniform radial microstructures of different heat-patterns on the mechanical properties, microhardness test and tensile test were conducted. The Vickers microhardness test was conducted on the surface of heat-

patterns using a Struers Duramin-A300 hardness machine to get microhardness distribution maps, with the load as 200 g and dwell time as 10 s. The room temperature tensile test was conducted on a tensile test machine (INSTRON 3382) with a cross-head speed of 1 mm/min. Fig.4 shows the detailed dimensions and configuration of the joint and sliced samples for tensile test.

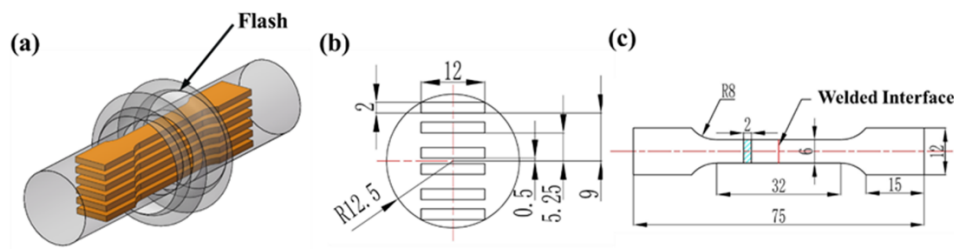


Fig.4 Structure and dimensions of samples used to study radial mechanical properties of joint showing (a) schematic diagram of slicing, (b) slicing position and (c) dimensions of the tensile sample

### 3. Results

#### 3.1 Heat-patterns of Ti-6Al-4V joint

To obtain diverse heat-patterns, RFW experiments were undertaken at varied rotational speeds. Fig.5 shows the appearances of Ti-6Al-4V joints welded at different rotational speeds, which can be distinguished from the flash appearances in general. Sticky flashes appear at joints formed between 500 and 1200 rpm, while extruded flashes appear between 1500 and 1800 rpm. Distinct flashes at the contact indicate different residual plasticized metals, the morphology of which is HP.

Fig.6 depicts heat-patterns of Ti-6Al-4V joints welded at various rotational speeds, which can be separated into two types. HP created with a sticky flash at 500rpm to

1200rpm has a morphology that resembles a pair of glasses, which is significantly distinct from the common varieties of HP illustrated in Fig.1. Whereas, HP produced from 1500rpm to 1800rpm with an extruded flash has a common 'scissor-like' or 'X-like' morphology, as previously reported. As a result, during RFW, the rotational speed causes HP fluctuations in the Ti-6Al-4V joint, which will be detailed in section 4.1.

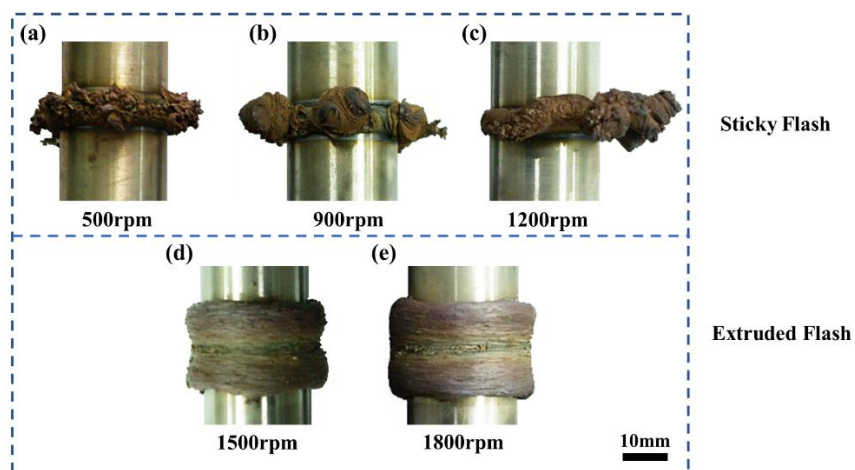


Fig.5 Appearances of Ti-6Al-4V joint welded at (a) 500rpm, (b) 900rpm, (c) 1200rpm, (d) 1500rpm and (e) 1800rpm

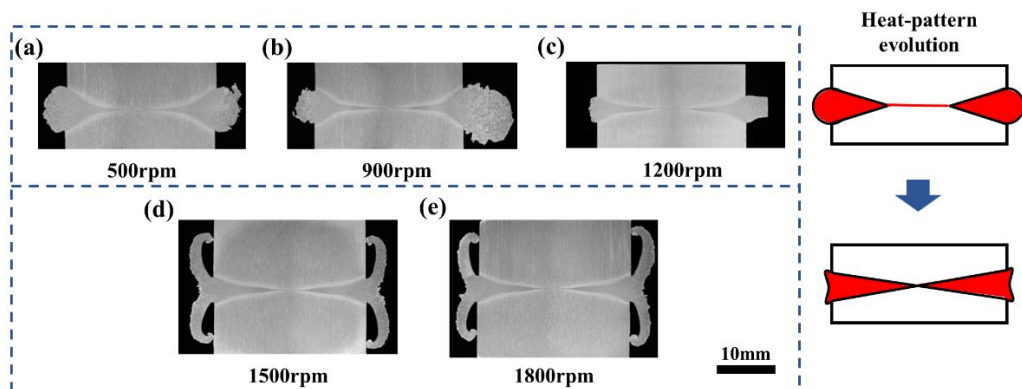


Fig.6 Heat-patterns of Ti-6Al-4V joint welded at (a) 500rpm, (b) 900rpm, (c) 1200rpm, (d) 1500rpm and (e) 1800rpm

### 3.2 Non-uniform radial microstructures inner heat-patterns

Heat-patterns of Ti-6Al-4V rotary friction welded joint are generally described as

two variations, the 'glass - like' pattern and the 'scissor - like' pattern. The radial microstructures of 'glass-like' HP and 'scissor-like' HP were then investigated and characterized using joints welded at 500rpm and 1800rpm, respectively. Microstructures at center, 1/2R (R demonstrates the radius) and periphery were examined by SEM to get an overview of the radial microstructure distribution. Fig.7 shows the results of 'glass - like' Ti-6Al-4V HP welded at 500rpm. Generally, from center zone to the periphery, the microstructures evolve from equiaxed  $\alpha$  grains  $\rightarrow$  equiaxed  $\alpha$  grains and lamellar  $\alpha'$  laths  $\rightarrow$  lamellar  $\alpha'$  laths at center, 1/2R and periphery respectively. Fig.8 depicts the results of a 'scissor-like' Ti-6Al-4V HP welded at 1800rpm, whose radial microstructure distribution resembles that of a 'glass-like' HP. To be unusual,  $\alpha'$  colony forms at periphery of a 'scissor-like' HP.

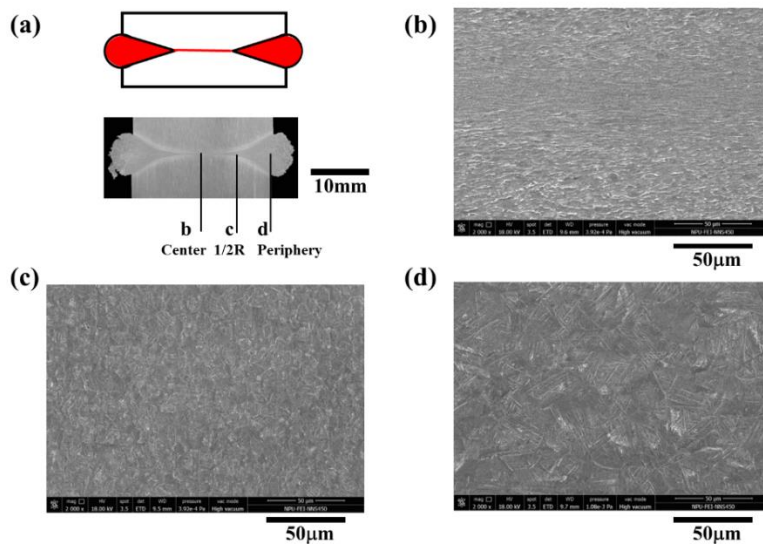


Fig.7 SEM images of 'glass - like' Ti-6Al-4V HP welded at 500rpm in different zones: (a) the morphology, (b) center zone, (c) zone at 1/2R and (d) zone at periphery

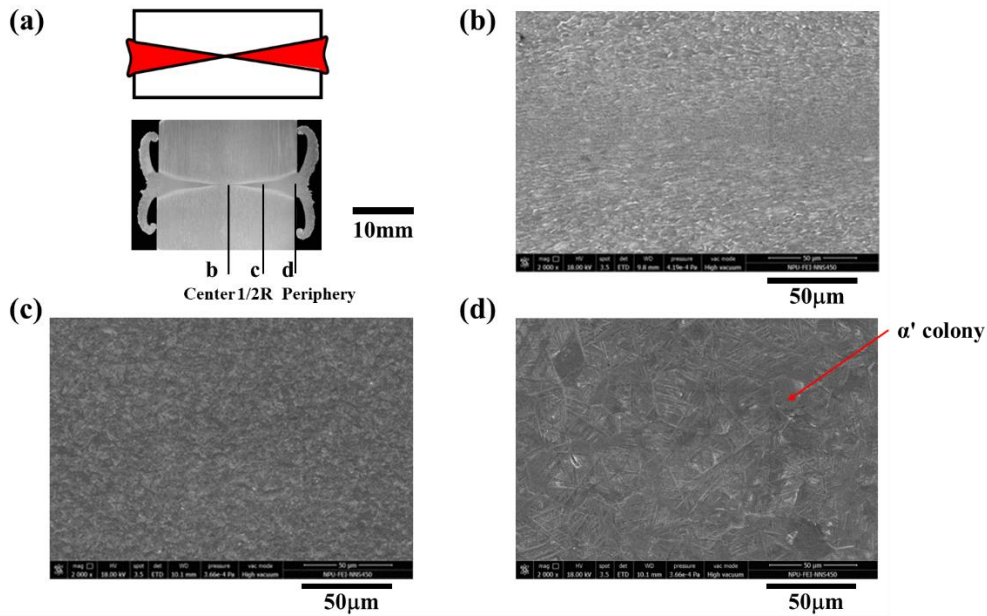


Fig.8 SEM images of 'scissor - like' Ti-6Al-4V HP welded at 1800rpm in different zones: (a) the morphology, (b) center zone, (c) zone at 1/2R and (d) zone at periphery

EBSD was then employed to study five highlighted zones along the welded line to further describe the radial microstructures inner heat-patterns. The findings of a 'glass-like' Ti-6Al-4V HP welded at 500rpm are shown in Fig.9. The bcc  $\beta$  phase is marked as white, which shows neglectable effect on the microstructures. On the other hand, the morphology and size of  $\alpha$  phase vary at different zones. Along the welded line, the radial microstructure evolves from equiaxed  $\alpha$  grains to lamellar  $\alpha'$  laths from center to periphery, where the fraction of equiaxed  $\alpha$  grains declines as the proportion of lamellar  $\alpha'$  laths grows. Furthermore, the lamellar  $\alpha'$  lath develops in size from the center to the periphery. The results of a 'scissor-like' Ti-6Al-4V HP welded at 1800rpm, with a radial microstructure distribution similar to that of a 'glass-like' HP, are shown in Fig.10. To be unusual,  $\alpha'$  colony arises at periphery of a 'scissor-like' HP.

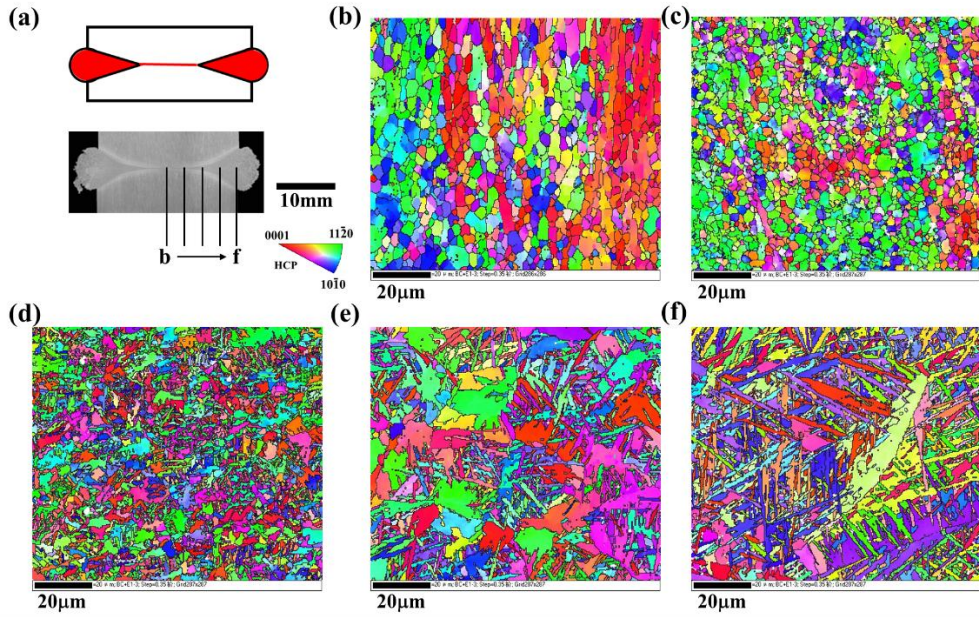


Fig.9 Radial microstructures of 'glass - like' Ti-6Al-4V HP welded at 500rpm showing (a) the morphology and IPF maps at different positions in radial direction from (b) to (f)

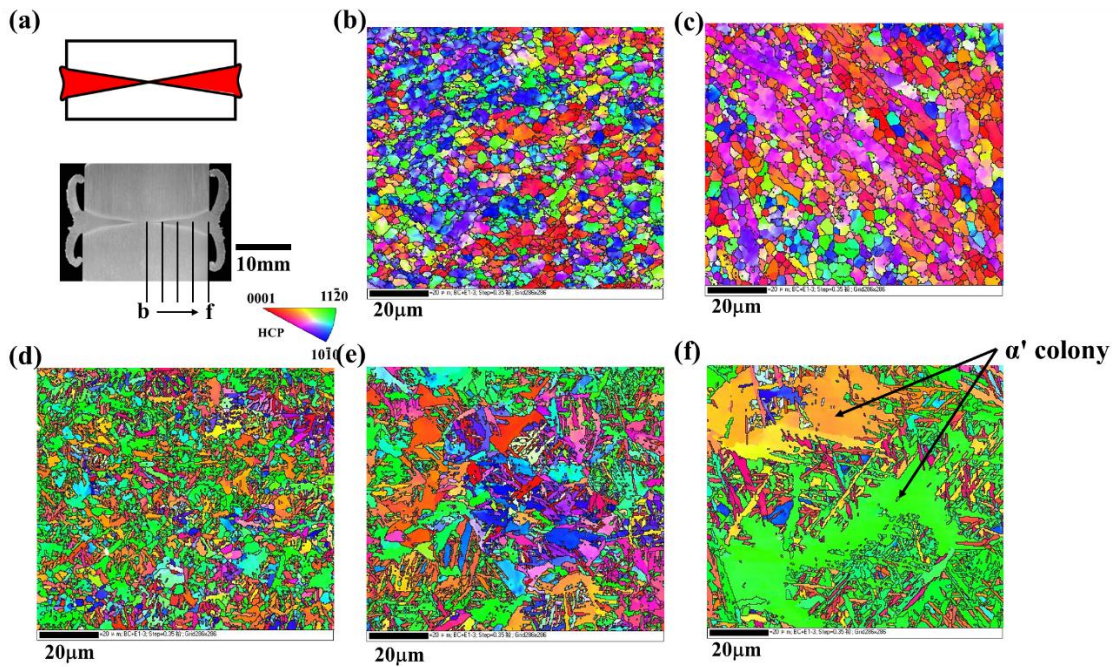


Fig.10 Radial microstructures of 'scissor - like' Ti-6Al-4V HP welded at 1800rpm showing (a) the morphology and IPF maps at different positions in radial direction

from (b) to (f)  
14

### 3.3 Non-uniform radial mechanical properties

Fig.11 shows the microhardness distribution maps of Ti-6Al-4V joint welded at 500rpm and 1800rpm corresponding to ‘glass - like’ HP and ‘scissor - like’ HP respectively. Generally, the distribution of microhardness at the interface is characterized by a high center and a low periphery. According to the results of radial microstructure shown above, equiaxed  $\alpha$  grains formed at center is harder than the lamellar  $\alpha'$  laths at periphery. Comparing the hardness distribution of two different heat-patterns, the ‘scissor - like’ HP has a lower hardness at periphery, which indicates that the formation of  $\alpha'$  colony will further reduce the hardness.

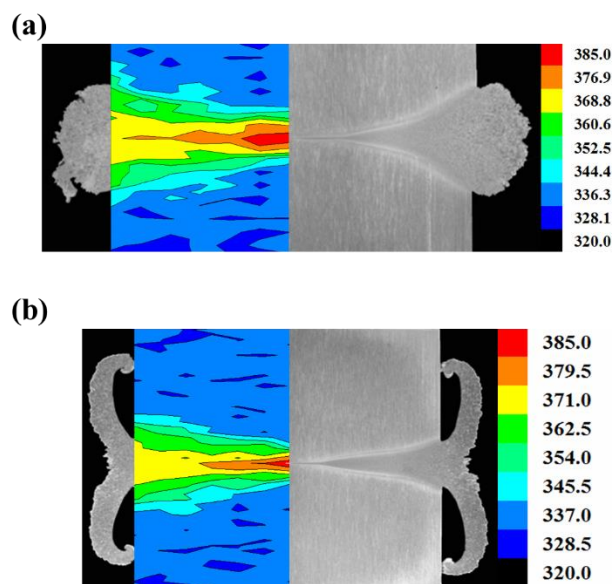


Fig.11 Microhardness distribution maps of Ti-6Al-4V joint welded at (a) 500rpm and (b) 1800rpm corresponding to ‘glass - like’ HP and ‘scissor - like’ HP respectively

Tensile tests were then conducted to investigate the effect of the non-uniform radial microstructures on the properties. The sliced samples (shown in Fig.4) at 0.04R-0.2R, 0.42R-0.58R and 0.72R-0.88R (R demonstrates the radius) were employed to test and characterize the properties of center, 1/2R and periphery. Fig.12 shows a clear

variability in the radial tensile properties of the joint, where the central zone has a higher strength and elongation compared with the periphery. The strength distribution is relatively uniform, which is close to or even slightly higher than the base metal (BM). As an example, the center strength of 'glass - like' HP is 994MPa and periphery is 965MPa, which are both slightly higher than 963MPa of base metal. The periphery strength of 'scissor - like' HP is 954MPa, which is close to the strength of the base metal. It is a common feature that the strength of friction welded Ti-6Al-4V joint is close to or even higher than the base metal [32,33]. The refined microstructure formed at the interface ensures the strength of the joint. However, the elongation of the joint from center to periphery shows the distribution characteristics of high center and low periphery, which are quite lower than 16.1% of the base metal. The elongation of 'glass - like' HP is reduced from 13% (80.7% of base metal) at center to 10% (62.1% of base metal) at periphery, which is reduced nearly by 20%. Aggravating the issue further, the elongation of 'scissor - like' HP is reduced from 13.1% (81.4% of base metal) at center to 8.1% (50.3% of base metal) at periphery, which is reduced by 31.1%. This result means that the formation of lamellar  $\alpha'$  laths at periphery will significantly reduce the plasticity of the joint. At center, the microstructure is dominated by equiaxed  $\alpha$ , which is consistent with the base metal. Therefore, the overall microstructure is thought to be more uniform so that generates better elongation. The formation of lamellar  $\alpha'$  laths at periphery makes the difference between interfacial microstructure and the base metal, so the plasticity is reduced. To aggravates this issue,  $\alpha'$  colony arises at periphery of the 'scissor-like' HP further reduces the plasticity.

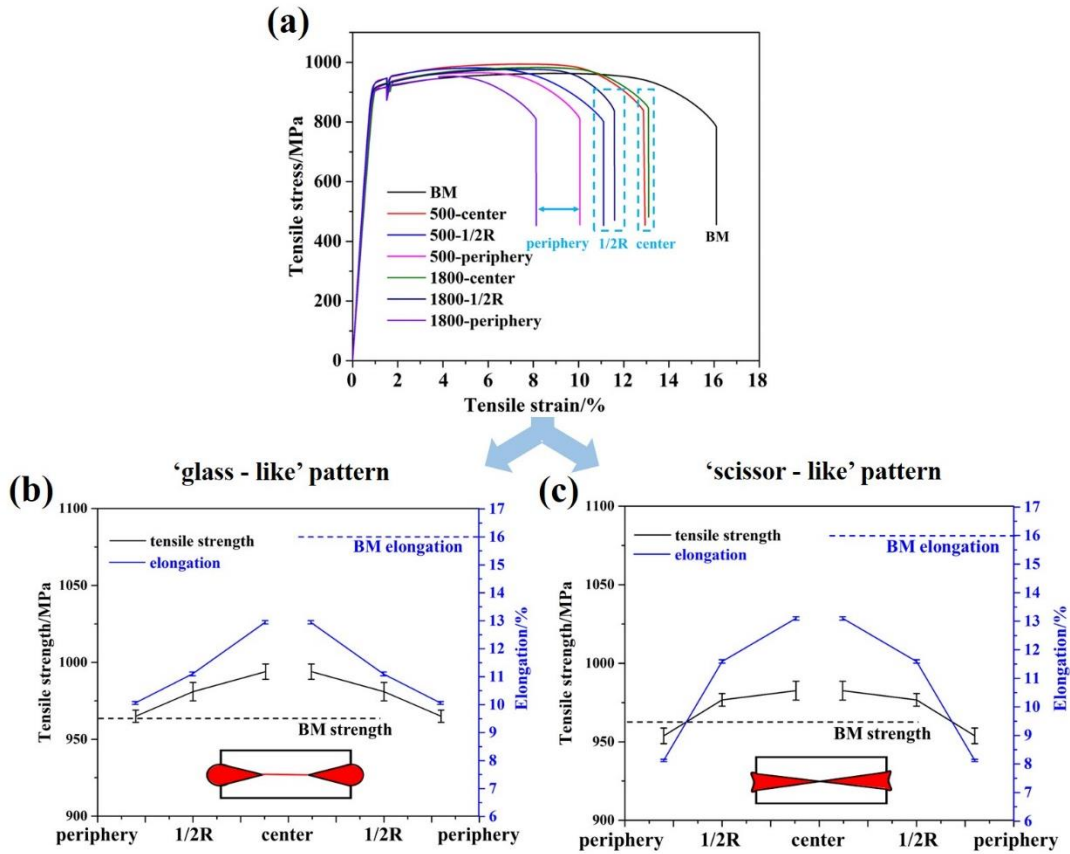


Fig.12 Non-uniform radial tensile strength and elongation of different Ti-6Al-4V heat-patterns showing (a) stress-strain curves, (b) radial properties of ‘glass-like’ HP welded at 500rpm and (c) radial properties of ‘scissor-like’ HP welded at 1800rpm

#### 4. Discussion

Generally, ‘glass-like’ HP and ‘scissor-like’ HP of Ti-6Al-4V are formed at various rotational speeds. The microstructure inner HP of the joint is varied along the radial direction, which results in non-uniform radial mechanical properties. In this section, simulation was used to clarify the formation mechanism of different heat-patterns.  $\beta$ -reconstruction was at first time employed to understand the underlying mechanisms leading to the varied radial microstructures of a titanium friction welded joint. Finally, the relationship between radial microstructure and mechanical properties was analyzed.

## 4.1. Numerical modeling and formation mechanism of heat-patterns

### 4.1.1 Simulation model and settings

To prepare the data for clarifying the formation mechanism of different heat-patterns, a two-dimensional (2D) axisymmetric finite element (FE) model was developed using DEFORM to acquire the temperature field, axial stress field, and extrusion speed distribution. Fig.13 depicts a schematic representation of the axisymmetric model and mesh geometry. The quadrilateral mesh was divided into two halves due to the extreme deformation along the contact. Mesh at the friction interface was planned to be 0.3mm in size, corresponding to a length of 13mm, whereas mesh further from the interface was designed to be 2mm in size. The remeshing technique is available in DEFORM to avoid excessive mesh distortion in the process. For the analysis of RFW, isotropic material properties throughout the process, as well as temperature-dependent physical, thermal, and mechanical parameters, were assumed.

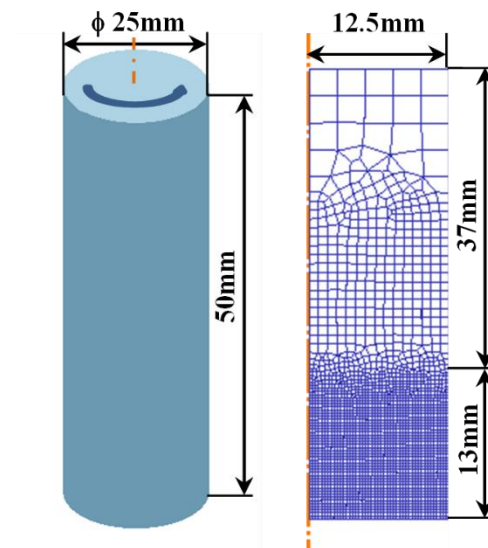


Fig.13 Schematic view of 2-D axisymmetric model and mesh geometry

To distinguish the friction behavior of Ti-6Al-4V in rotary friction welding under different rotational speeds, the friction torque was captured during RFW experiments to calculate nominal friction coefficient used in simulation. Fig.14 shows the evolution of friction coefficient at different rotation speeds. Then, according to the equation of friction torque (equation 1) and friction heat (equation 2), the heat generation can be obtained,

$$M = \frac{2}{3} \pi \mu P r^3 \quad (1)$$

$$q = \frac{2}{3} \mu P \omega r^3 \quad (2)$$

where  $M$  is the friction torque,  $q$  the friction heat,  $\mu$  the friction coefficient,  $P$  the welding pressure,  $\omega$  the friction angular velocity and  $r$  the friction radius.

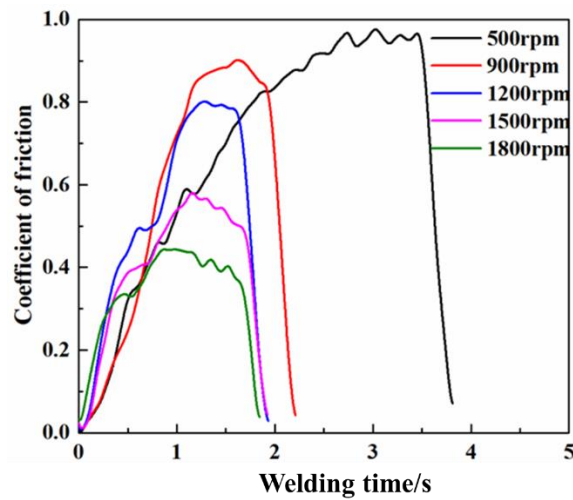


Fig.14 Evolution of friction coefficient at different rotation speeds

In order to improve the accuracy of the simulation results, the hyperbolic sinusoidal constitutive equation is used to describe the stress-strain relationship in friction welding process of Ti-6Al-4V [34]. The temperature-dependent properties specified for RFW of Ti-6Al-4V, i.e., thermal conductivity, Young's modulus, thermal expansion coefficient and specific heat and are listed in Table 2.

Table 2 The temperature-dependent properties of Ti-6Al-4V used in simulation

Temperature (°C)	20	200	400	600	800	1000	1200
Thermal conductivity (W/m·K)	6.9	8.7	10.3	13.1	15.2	17.4	19.5
Young's modulus (GPa)	114	104	94	74	—	—	—
Thermal expansion coefficient ( $10^{-6}\text{K}^{-1}$ )	9.0	9.2	9.5	10.0	—	—	—
Specific heat (J/kg·K)	610.1	653.2	690.7	712.3	719.8	724.9	729.4

The welding parameters were set as the same of RFW experiments. To investigate the formation mechanism of different heat-patterns, rotational speeds were set as 500rpm and 1800rpm, where the welding pressure was set as 40MPa and burn-off length 5mm.

#### 4.1.2 Experimental validation

Fig.15 shows the transition temperature fields of the joint welded at 500rpm corresponding to 'glass - like' HP. The high temperature contours initiate at periphery, spread inside and finally concentrate itself at periphery, which is corresponding to the morphology of 'glass - like' HP. Whereas, the high temperature contours of the joint welded at 1800rpm extrude itself to be the flash as shown in Fig.16, which is corresponding to the morphology of 'scissor - like' HP. The accuracy of the model is further validated by comparing the thermal cycle at the joint surface of simulation with the experiment monitored by infrared camera and the axial shortening curve obtained by simulation with the experiment captured by high-speed camera. Fig.17 and Fig.18 show the results of the joint welded at 500rpm and 1800rpm respectively, which are in

good agreement. These results confirm the 2D model that focuses on Ti-6Al-4V RFW process could simulate it well. Thereafter, the extrusion speed distribution and axial stress fields were used to clarify the formation mechanism of different heat-patterns.

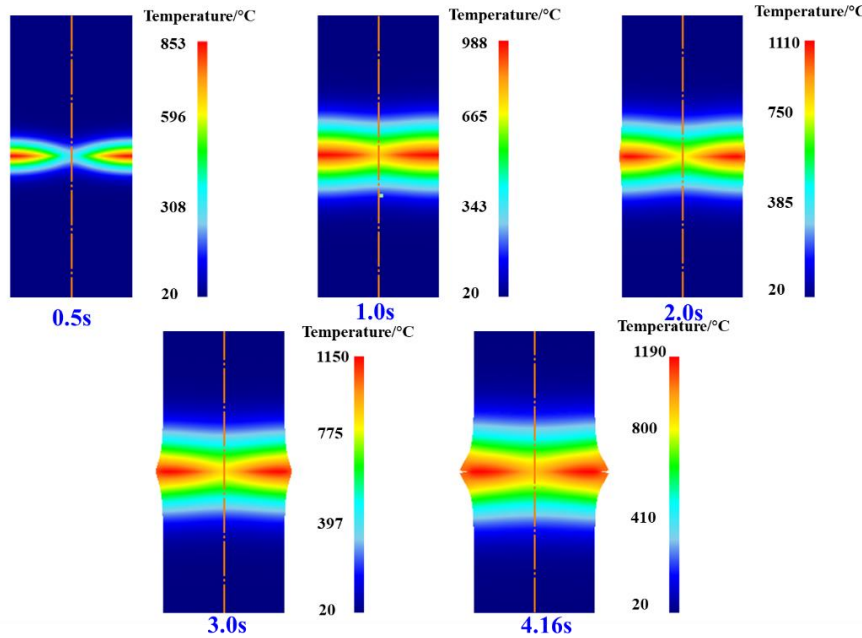


Fig.15 The transition temperature fields of the joint welded at 500rpm

corresponding to 'glass - like' HP

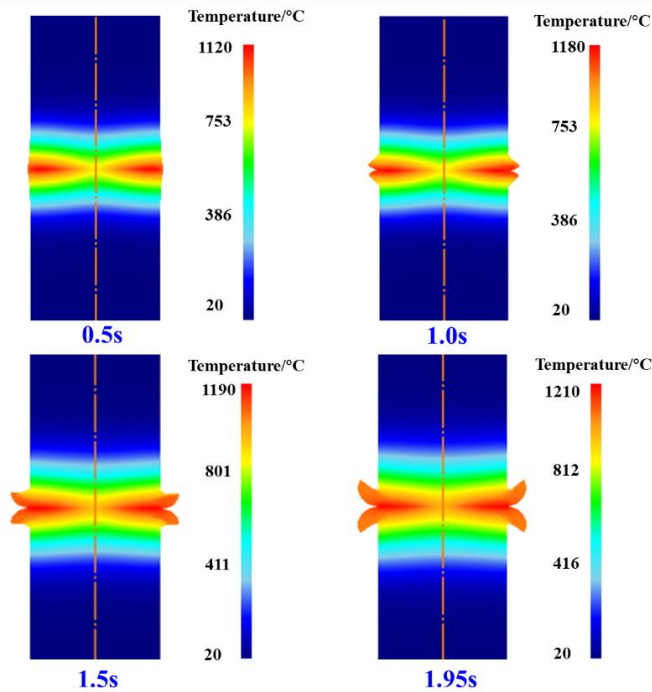


Fig.16 The transition temperature fields of the joint welded at 1800rpm

corresponding to 'scissor - like' HP

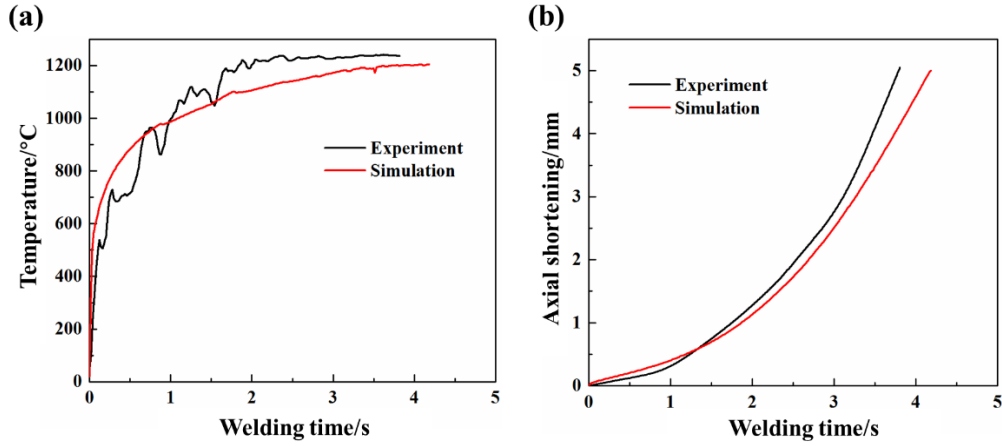


Fig.17 Comparisons of (a) thermal cycle at the joint surface of simulation with the experiment monitored by infrared camera and (b) axial shortening curve obtained by simulation with the experiment captured by high-speed camera welded at 500 rpm

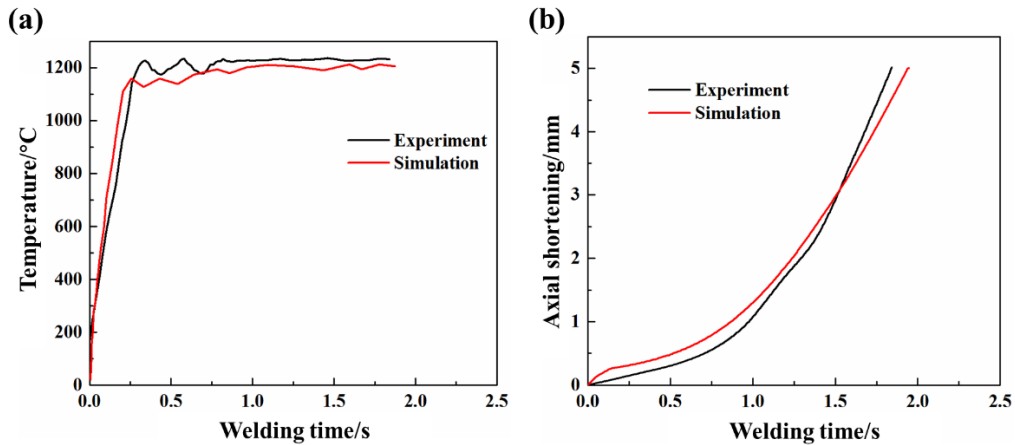


Fig.18 Comparisons of (a) thermal cycle at the joint surface of simulation with the experiment monitored by infrared camera and (b) axial shortening curve obtained by simulation with the experiment captured by high-speed camera welded at 1800 rpm

#### 4.1.3 Formation mechanism of Ti-6Al-4V heat-patterns

Fig.19 shows the extrusion speed distribution of plasticized metal in radial direction. Fig.19a shows the extrusion speed of 'glass-like' HP concentrates at the

sticky flash which indicates that the plasticized metal formed at friction interface will flow to the flash zone. Whereas Fig.19b shows the extrusion speed of ‘scissor-like’ HP concentrates at the interface near periphery that indicates the plasticized metal will flow to periphery. Furthermore, the plasticized metal will be extruded to be flash under the function of axial tensile stress. Fig.20 shows the transition stress-Z fields of ‘glass - like’ HP, whose axial tensile stress (0.537MPa) isn’t enough to flip the flash when it initiates at about 2.0s considering accumulated plasticized metal. Whereas, the axial tensile stress (0.773MPa) is enough to flip the flash when it initiates of ‘scissor - like’ HP. In summary, the joint welded at 500rpm squeezes the interfacial plasticized metal towards and accumulated at periphery, where the axial tensile stress isn’t enough to flip the metal into extruded flash. Therefore, the ‘glass - like’ HP is formed which consumes more welding time (~4s) to squeeze the interfacial plasticized to be stick flash to achieve a burn-off of 5mm. Whereas, the joint welded at 1800rpm extrudes the plasticized metal into flash which consumes less welding time (~2s) to achieve 5mm burn-off. As a result, ‘scissor - like’ HP is formed.

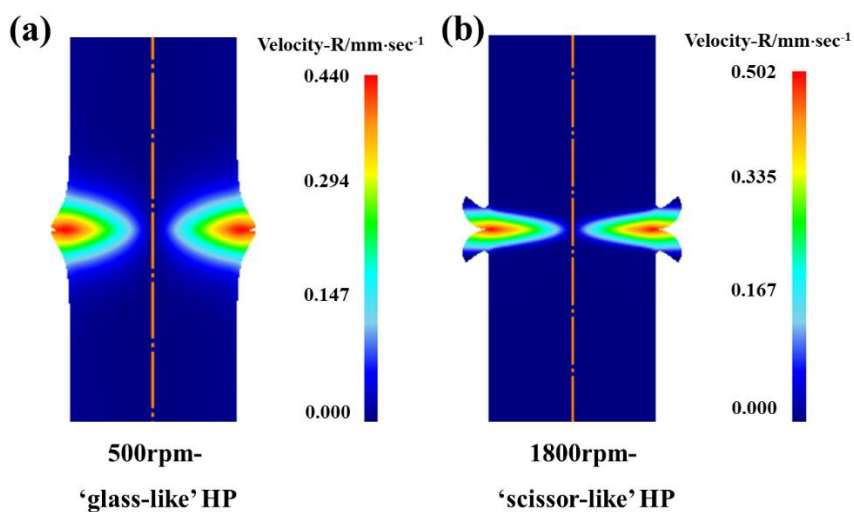


Fig.19 Extrusion speed distribution of plasticized metal in radial direction at rotational

speed of (a) 500rpm and (b) 1800rpm

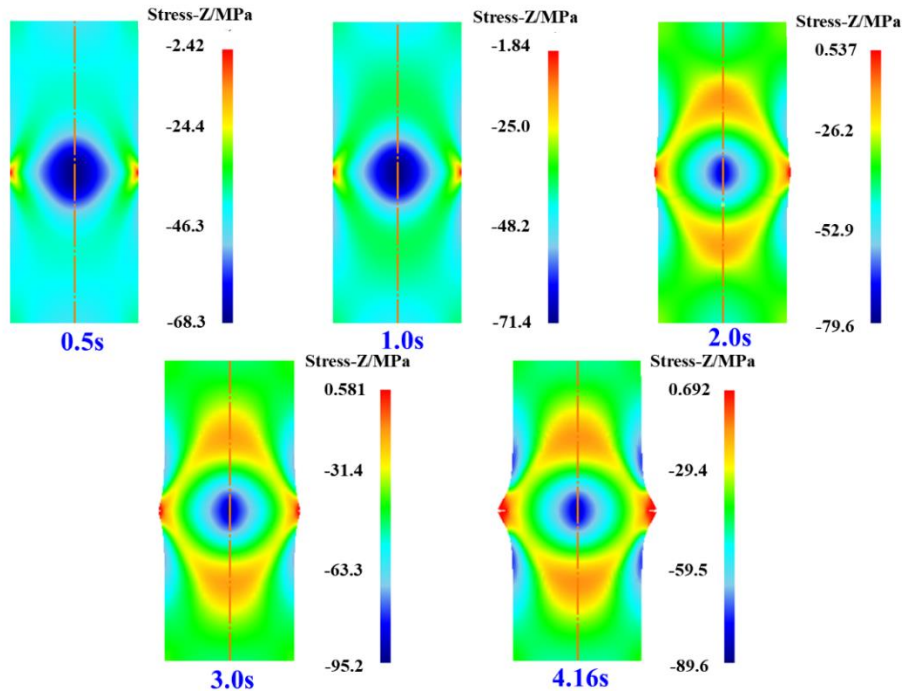


Fig.20 The transition stress-Z fields of the joint welded at 500rpm

corresponding to 'glass - like' HP

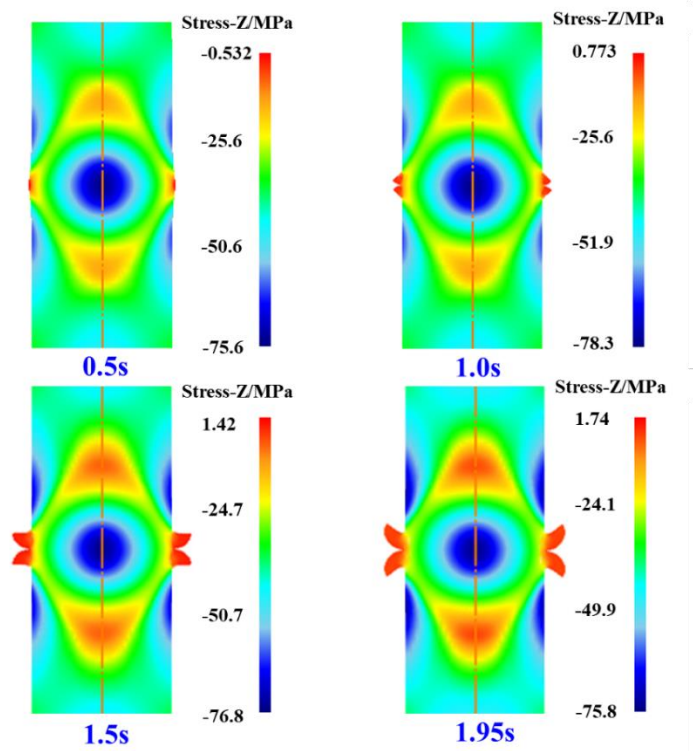


Fig.21 The transition stress-Z fields of the joint welded at 1800rpm

corresponding to 'glass - like' HP

## 4.2 Mechanism leading to the varied radial microstructures

' $\beta$ -reconstruction' was at first time used to exactly identify the  $\beta$  grains and remaining equiaxed  $\alpha$  grains to clarify the mechanism leading to the varied radial microstructures of Ti-6Al-4V heat-pattern. ' $\beta$  grains' at welding temperature, which cannot be observed and characterized directly at room temperature, were reconstructed according to inherent  $\alpha$  orientations shown in Fig.9 and Fig.10. Fig.22 shows  $\beta$ -reconstruction results of radial microstructures of 'glass - like' Ti-6Al-4V HP based on the EBSD results in Fig.9, where  $\beta$  grains are marked in IPF maps and equiaxed  $\alpha$  grains are marked in white. Generally, the content of  $\beta$  increases from center to periphery with size growth. Thereafter, the  $\beta$  grains (at welding temperature) will transit into lamellar  $\alpha'$  laths during the cooling process after welding, where  $\beta$  grains with large sizes will form large and thick lamellar  $\alpha'$  laths. Therefore, equiaxed  $\alpha$  grains are predictable to govern the center zone (Fig.22b, 22c) since few  $\beta$  grains are formed in welding process. Deformation of equiaxed  $\alpha$  grains is the main mechanism at center zone during the welding process. The recrystallized distribution map show in Fig.23 further confirms this issue. As seen in Fig.23b and 23c, deformed grains and sub-grains dominate this area (center zone). At 1/2R, most of the equiaxed  $\alpha$  grains in base metal phase transition into  $\beta$  grains during the welding process. Therefore, the microstructure at 1/2R of the joint is consisted of remaining deformed equiaxed  $\alpha$  grains (shown in Fig.23d) and lamellar  $\alpha'$  laths transit from  $\beta$  grains during the cooling process. Whereas, equiaxed  $\alpha$  grains of the base metal at periphery almost transition into  $\beta$  grains with

large size, shown in Fig.22e and 22f. As has been discussed above, ‘glass-like’ HP concentrates the frictional heat and plasticized metal at periphery with a comparatively long welding time. Therefore,  $\beta$  grains of ‘glass-like’ HP at periphery grow into a larger size. Long and thick lamellar  $\alpha'$  laths therefore are formed from large  $\beta$  grains during the cooling process.

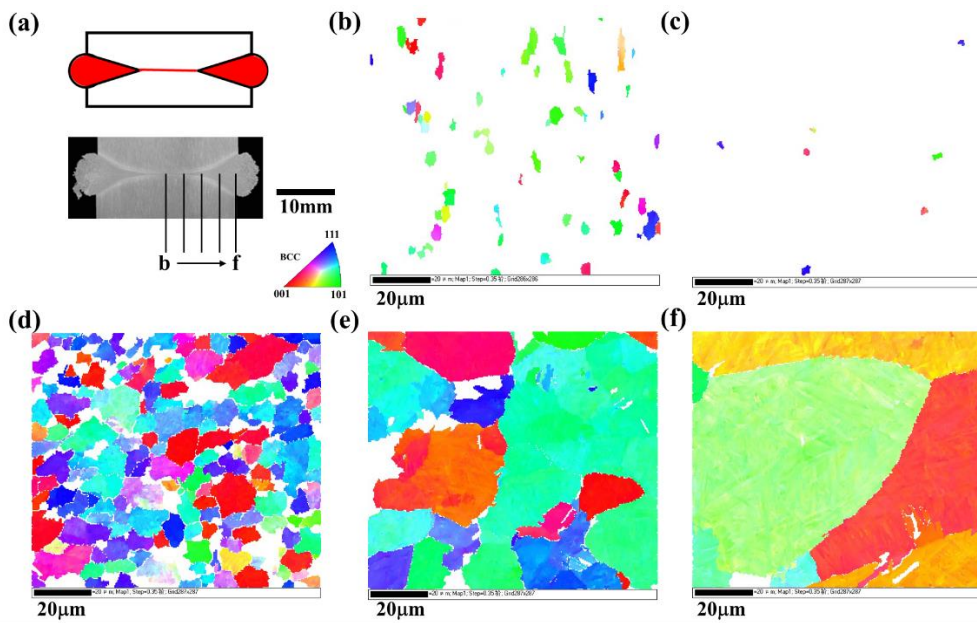


Fig.22  $\beta$ -reconstruction results of radial microstructures of ‘glass - like’ Ti-6Al-4V HP welded at 500rpm showing (a) the morphology and  $\beta$ -reconstruction IPF maps at different positions in radial direction from (b) to (f)

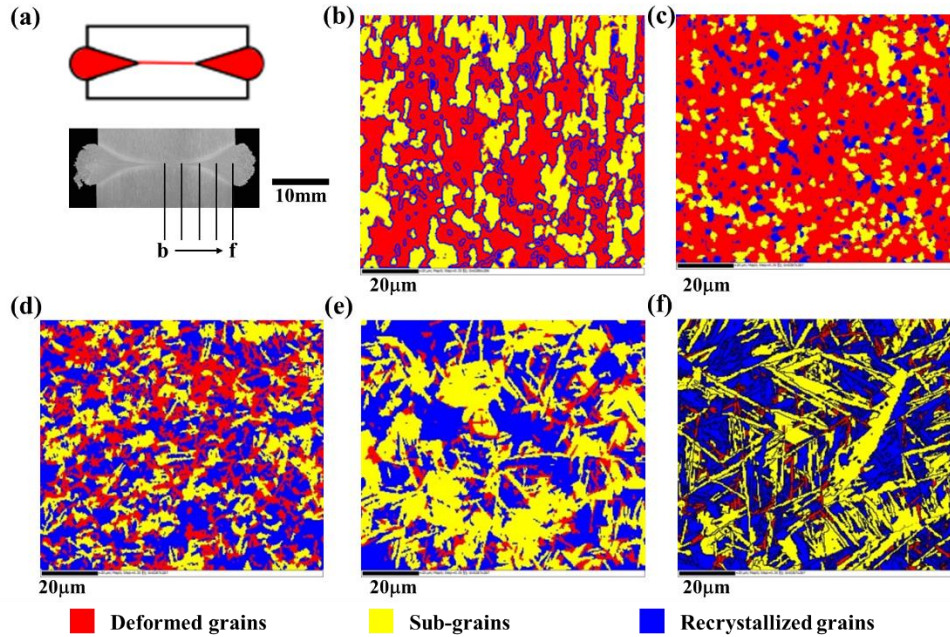


Fig.23 Recrystallized distribution map of radial microstructures of ‘glass - like’

Ti-6Al-4V HP welded at 500rpm

The radial microstructures of ‘scissor - like’ HP and the corresponding formation mechanisms are similar to that of ‘glass - like’ HP, as shown in Fig.24 and Fig.25. To be different,  $\alpha'$  colony arises at periphery of 'scissor-like' HP. Fig.24 shows  $\beta$ -reconstruction results of radial microstructures of ‘scissor-like’ Ti-6Al-4V HP based on the EBSD results in Fig.10. As one may noticed, the large  $\beta$  grains (at welding temperature) at periphery shown in Fig.24e and 24f trend to be  $\langle 111 \rangle$  crystallographic orientation, which may be related to the radial extrusion of the plasticized material. Comparatively speaking, plasticized metal at periphery of ‘glass - like’ HP have undergone a long welding time to rotate to various orientations. Whereas, plasticized metal at periphery of ‘scissor - like’ HP corresponds to the metal in the continuous extrusion process (short time), where the excess metal is extruded to be the flash. The  $\beta$  grains with the similar orientation will form lamellar  $\alpha'$  laths with similar orientation,

which is named as  $\alpha'$  colony.

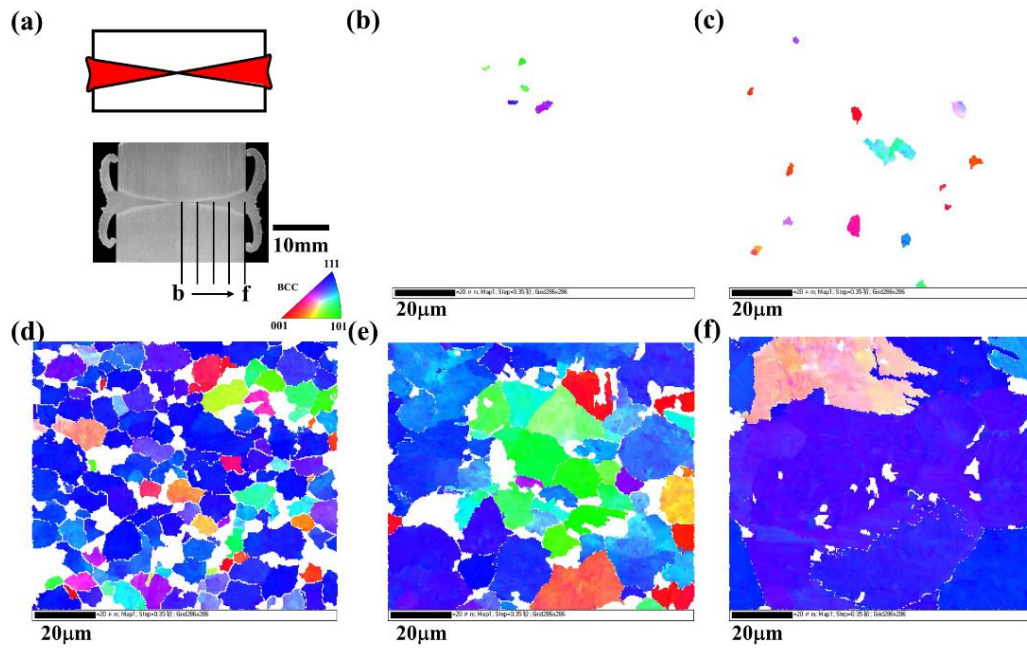


Fig.24  $\beta$ -reconstruction results of radial microstructures of 'scissor - like' Ti-6Al-4V HP welded at 1800rpm showing (a) the morphology and  $\beta$ -reconstruction IPF maps at different positions in radial direction from (b) to (f)

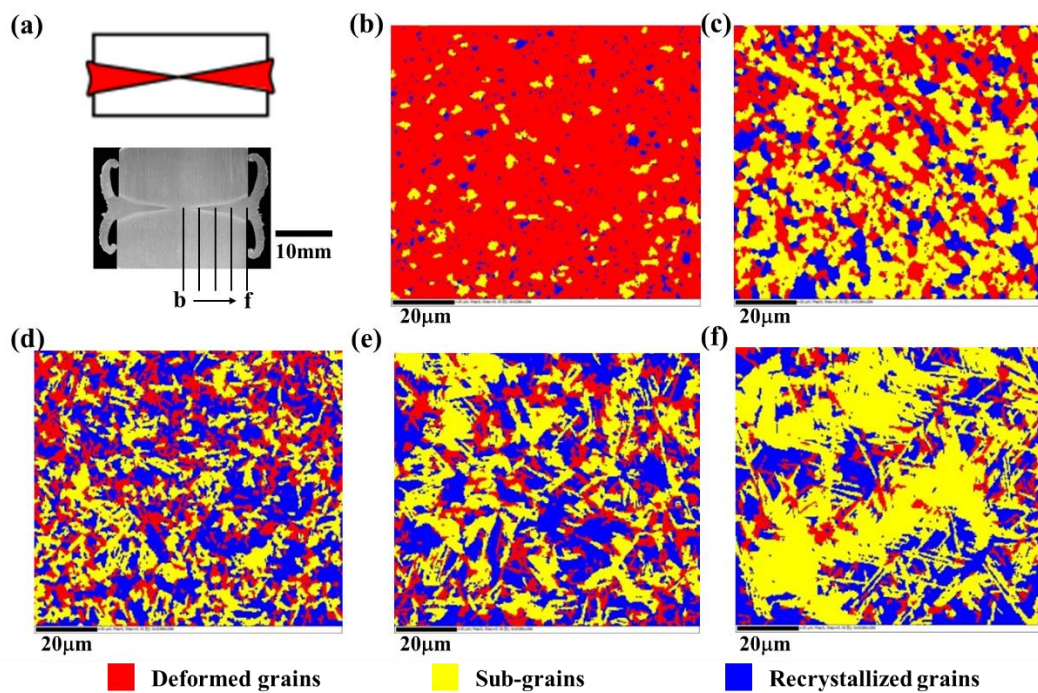


Fig.25 Recrystallized distribution map of radial microstructures of 'scissor - like'

Ti-6Al-4V HP welded at 1800rpm

### 4.3 Relationship between microstructure and mechanical properties

HP is the result of the comprehensive effect of many factors, such as frictional heat distribution, plastic flow and axial stress distribution. The formation of HP leads to the non-uniform radial microstructure and properties of Ti-6Al-4V joint, which has been summarized in Fig.26. For the 'glass-like' HP, the plasticized metal at the interface is extruded and concentrated at periphery. According to the results of  $\beta$ -reconstruction, the radial microstructures of 'glass-like' HP are deformed  $\alpha$  grains  $\rightarrow$  deformed  $\alpha$  grains and lamellar  $\alpha'$  laths  $\rightarrow$  lamellar  $\alpha'$  laths corresponding to center  $\rightarrow$  1/2R  $\rightarrow$  periphery respectively. Deformed  $\alpha$  grains at center zone make the strength higher than that of BM. Meanwhile, deformed  $\alpha$  grains share the similar morphology of equiaxed  $\alpha$  grains of base metal compared with the lamellar  $\alpha'$  laths at 1/2R and periphery, which indicates the axial structure is relatively uniform. Therefore, the elongation at center is the highest among the three regions of center, 1/2R and periphery, reaching 80.7% of BM. Whereas, lamellar  $\alpha'$  laths at periphery share a coarser size than that of the center zone, the strength of which is reduced and close to the BM. Compared with the deformed  $\alpha$  grains, lamellar  $\alpha'$  laths are quite different from equiaxed  $\alpha$  grains of BM in morphology, which causes a significant reduction in elongation. The elongation at periphery is only 62.1% of base metal, which is reduced by nearly 20% to that of the center zone. Microstructure at 1/2R is the mixture of deformed  $\alpha$  grains and lamellar  $\alpha'$  laths, whose strength and elongation are therefore lower than that of center zone but higher than the periphery. For 'scissor-like' HP, its radial microstructure and properties distribution are similar to those of 'glass-like' HP. To be different, lamellar  $\alpha'$  laths at

periphery of ‘scissor-like’ HP have similar orientations, which form  $\alpha'$  colony. The formation of  $\alpha'$  colony further increases the difference in morphology between the welded zone and BM, significantly reducing the elongation, which is only 50.3% of BM, reduced by nearly 31.1% to that of the center zone.

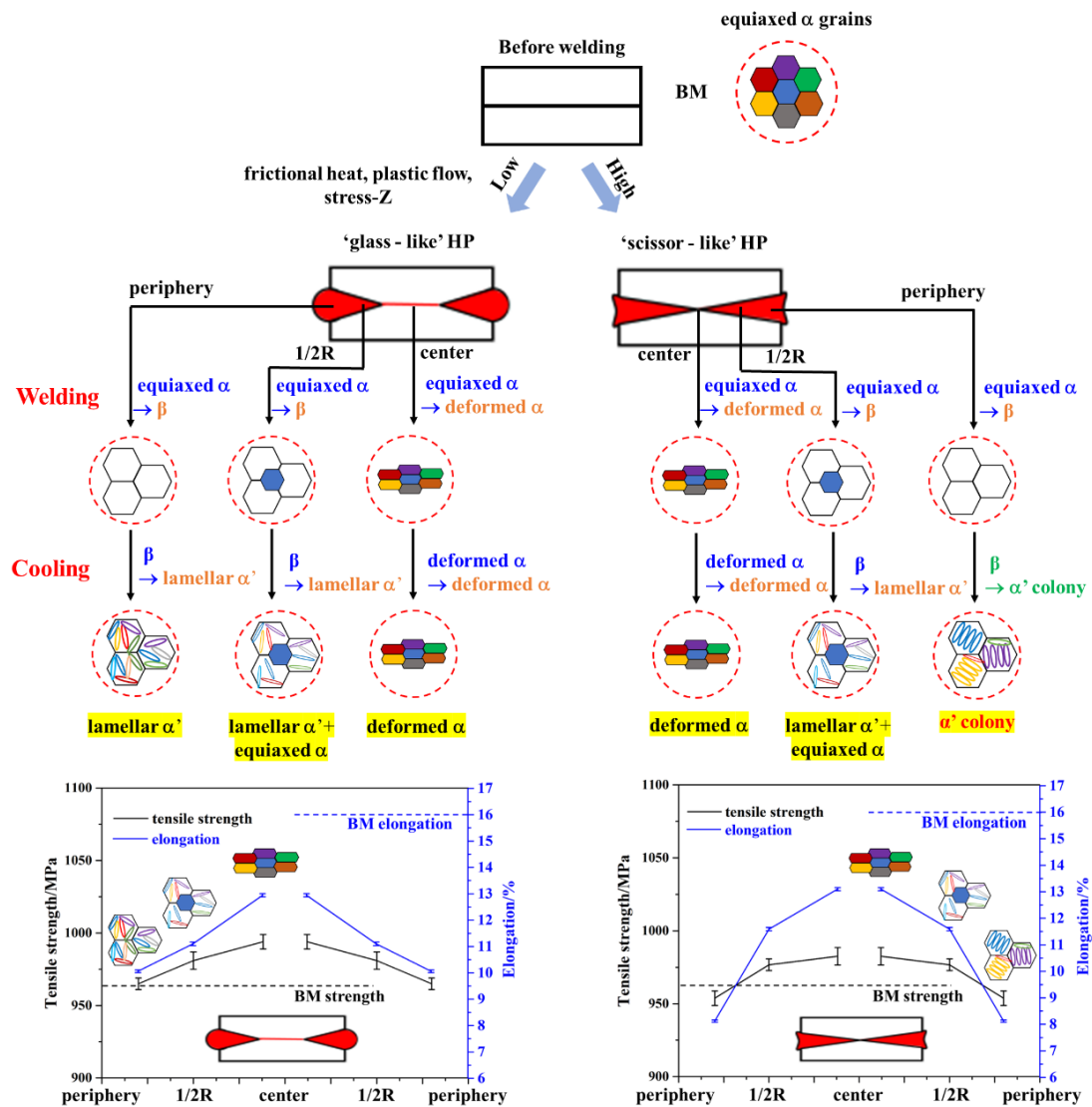


Fig.26 Heat-pattern induced non-uniform radial microstructure and properties of Ti-6Al-4V joint

## 5. Conclusions

Heat-pattern of Ti-6Al-4V rotary friction welded joint was focused in this study.

RFW experiments were carried out at various rotational speeds to acquire varied heat-patterns, the formation mechanism of which was clarified by simulation results. Then, heat-pattern induced non-uniform radial microstructure and properties were investigated.  $\beta$ -reconstruction was at first time employed to clarify the formation of non-uniform radial microstructures. The effects of non-uniform radial microstructures of different heat-patterns on the mechanical properties were analyzed. The following conclusions were drawn:

- (1) Heat-patterns of Ti-6Al-4V joints welded at different rotational speeds can be generally separated into two variations, 'glass-like' HP and 'scissor-like' HP. HP created with a sticky flash at 500rpm to 1200rpm has a morphology that resembles a pair of glasses, which is named as 'glass-like' HP. Whereas, HP produced from 1500rpm to 1800rpm with an extruded flash has a 'scissor-like' morphology, which is named as 'scissor-like' HP.
- (2) At low rotational speeds (i.e., 500rpm-1200rpm), the joint squeezes the interfacial plasticized metal towards and accumulated at periphery, where the axial tensile stress isn't enough to flip the metal into extruded flash. Therefore, the 'glass-like' HP is formed. Whereas, the joint welded at 1500rpm to 1800rpm concentrates the extrusion speed at the interface near periphery to make the plasticized metal will flow to periphery. Under the function of axial tensile stress, the plasticized metal is extruded to be flash to form 'scissor-like' HP.
- (3) HP induces non-uniform radial microstructures, the formation mechanism of which were clarified by  $\beta$ -reconstruction. According to the results of  $\beta$ -reconstruction, the

radial microstructures of 'glass-like' HP are deformed  $\alpha$  grains  $\rightarrow$  deformed  $\alpha$  grains and lamellar  $\alpha'$  laths  $\rightarrow$  lamellar  $\alpha'$  laths corresponding to center  $\rightarrow$  1/2R  $\rightarrow$  periphery respectively. For 'scissor-like' HP, its radial microstructure distribution are similar to those of 'glass-like' HP. To be different, lamellar  $\alpha'$  laths at periphery of 'scissor-like' HP have similar orientations, which form  $\alpha'$  colony.

- (4) The non-uniform radial microstructures cause non-uniform radial properties. Deformed  $\alpha$  grains at center zone make the strength higher than that of BM and share the similar morphology of BM compared with the lamellar  $\alpha'$  laths to get the highest elongation among the three regions of center, 1/2R and periphery, reaching 80.7% of BM. Whereas, lamellar  $\alpha'$  laths at periphery share a coarser size than that of the center zone, the strength of which is reduced and close to the BM. Compared with the deformed  $\alpha$  grains, lamellar  $\alpha'$  laths are quite different from BM in morphology, which causes a significant reduction in elongation to only 62.1% of BM. Microstructure at 1/2R is the mixture of deformed  $\alpha$  grains and lamellar  $\alpha'$  laths, whose strength and elongation are therefore lower than that of center zone but higher than the periphery. For 'scissor-like' HP, its radial microstructure and properties distribution are similar to those of 'glass-like' HP. To be different, lamellar  $\alpha'$  laths at periphery of 'scissor-like' HP have similar orientations to form  $\alpha'$  colony, which further increases the difference in morphology between the welded zone and BM and therefore significantly reducing the elongation to only 50.3% of BM.

## Acknowledgements

This work was supported by the research fund of the National Natural Science Foundations of China (Grant Nos. 52205416, 52075551) and the China Postdoctoral Science Foundation (2021M692627), Shaanxi Talent Promotion Plan Youth Science and Technology Rising Star Project (2020KJXX-045). Feng Jin is grateful for financial support from the Chinese Scholarship Council (CSC 202106290001). The authors declare they have no conflict of interest.

## References

- [1] Dorick B, Salima B, Marion Risbet. Contributions of an innovative post-weld heat treatment to the micro-tensile behavior of two mono-material linear friction welded joints using: The  $\beta$ - metastable Ti-5Al-2Sn-2Zr-4Mo-4Cr (Ti17) and the near- $\alpha$  Ti-6Al-2Sn-4Zr-2Mo (Ti6242) Ti-alloys. *Materials Science and Engineering A*, 2019, 766:138334.
- [2] Wen G D, Ma T J, Li W Y, et al. Strain-controlled fatigue properties of linear friction welded dissimilar joints between Ti-6Al-4V and Ti-6.5Al-3.5Mo-1.5Zr-0.3Si alloys. *Materials Science and Engineering A*, 2014, 612 (7): 80-88.
- [3] Wang B, Chen X, Yang J, et al. Microstructural response at the interface and its effect on the fatigue fracture behavior of rotary friction welded dissimilar titanium alloys: Ti-5Al-2Sn-2Zr-4Mo-4Cr (Ti17) and Ti-6Al-2Sn-4Zr-2Mo (Ti6242). *Materials Research Express*, 2021, 8(10):106513.

- [4] Wang S Q, Li W Y, Zhou Y, et al. Tensile and fatigue behavior of electron beam welded dissimilar joints of Ti-6Al-4V and IMI834 titanium alloys. *Materials Science and Engineering A*, 2016, 649: 146-152.
- [5] Chen G, Zhang G, Yin Q, et al. Microstructure evolution of electron beam welded joints of Ti-43Al-9V-0.3Y and Ti-6Al-4V alloys. *Materials Letters*, 2018, 233: 336-339.
- [6] Jin F, Li J L, Liu P, et al. Friction coefficient model and joint formation in rotary friction welding. *Journal of Manufacturing Processes*, 2019, 46: 286-297.
- [7] Jin F, Li J L, Du Y J, et al. Numerical simulation based upon friction coefficient model on thermo-mechanical coupling in rotary friction welding corresponding with corona-bond evolution. *Journal of Manufacturing Processes*, 2019, 45: 595-602.
- [8] Li W Y, Vairis A, Preuss M, et al. Linear and rotary friction welding review. *International Materials Reviews*, 2016, 61(2):71-100
- [9] Chen H Y, Fu L, Zhang W Y, Liu F J. Radial Distribution Characteristics of Microstructure and Mechanical Properties of Ti-6Al-4V Butt Joint by Rotary Friction Welding. *Acta Metallurgica Sinica*, 2015, 28(10): 1291-1298.
- [10] Li X, Li J L, Liao Z X, Jin F, Xiong J T, Zhang F S. Effect of rotation speed on friction behavior and radially non-uniform local mechanical properties of AA6061-T6 rotary friction welded joint. *Journal of Adhesion Science and Technology*, 2018, 32(18): 1987-2006.

- [11]ASM International. ASM Handbook–Welding, Brazing and Soldering, Vol. 6. Materials Park, OH, 1993: 504-506, 508.
- [12]Udayakumar T, Raja K, Abhijit A T, Sathiya P. Experimental investigation on mechanical and metallurgical properties of super duplex stainless steel joints using friction welding process. Journal of Manufacturing Processes, 2013. 15(4): 558-571.
- [13]Li X, Li J L, Liao Z X, Jin F, Xiong J T, Zhang F S. Effect of rotation speed on friction behavior of rotary friction welding of AA6061-T6 aluminum alloy. Welding in the World, 2018, 62(5): 923-930.
- [14]Kimura M, Inoue H, Kusaka M, Kaizu K, Fuji A. Analysis method of friction torque and weld interface temperature during friction process of steel friction welding. Journal of Solid Mechanics and Materials Engineering, 2010, 4: 401-413.
- [15]Li P, Li J L, Li X, Xiong J T, Zhang F S, Liang L. A study of the mechanisms involved in initial friction process of continuous drive friction welding[J]. Journal of Adhesion Science and Technology, 2015, 29(12): 1246-1257.
- [16]Jin F, Li J L, Liao Z X, et al. The corona bond response to normal stress distribution during the process of rotary friction welding. Welding in the World, 2018, 62(5): 913-922.
- [17]Satyanarayana V G, Madhusudhan R, Mohandas T. Continuous drive friction welding studies on AISI 304 austenitic stainless steel welds. Materials and Manufacturing Processes, 2004, 19(3): 487-505.

- [18] Ajith P, Sathiya P, Aravindan S. Experimental Investigation on Friction Welding of UNS S32205 Duplex Stainless Steel. *Acta Metallurgica Sinica (English Letters)*, 2014, 27(6): 995-1007.
- [19] Ward A A, Zhang Y, Cordero Z C. Junction growth in ultrasonic spot welding and ultrasonic additive manufacturing. *Acta Materialia*, 2018, 158: 393-406.
- [20] Sun L X, Li M Q, Li H. Interface characteristics and recrystallization mechanism of dissimilar titanium bonds. *Journal of Materials Science*, 2018, 53:5380-5388.
- [21] Wang X Y, Li W Y, Ma T J, et al. Microstructural evolution and mechanical properties of a linear friction welded two-phase Ti-6.5Al-3.5Mo-1.5Zr-0.3Si titanium alloy joint. *Materials Science and Engineering A*, 2019, 743: 12-23.
- [22] Kim J, Murugan S, Kim J W, et al.  $\alpha/\beta$  phase transformation and dynamic recrystallization induced microstructure development in fine-grained Ti-6Al-4V friction stir weld. *Materials Characterization*, 2021, 178: 111300.
- [23] Alaborta E, Kontisb P, Barba D, et al. On the mechanisms of superplasticity in Ti-6Al-4V. *Acta Materialia*, 2016, 105: 449-463.
- [24] Seward G, Celotto S, Prior D J, et al. In situ SEM-EBSD observations of the hcp to bcc phase transformation in commercially pure titanium. *Acta Materialia*, 2016, 105: 449-463. 2004, 52(4): 821-832.
- [25] Humbert M, Wagner F, Moustahfid H, et al. Determination of the orientation of a parent  $\beta$  grain from the orientations of the inherited  $\alpha$  plates in the phase transformation from body-centred cubic to hexagonal close packed. *Journal of Applied Crystallography*, 1995, 28(5): 571-576.

- [26] Bachmann F, Hielscher R, Schaeben H. Texture analysis with MTEX–free and open source software toolbox//Solid State Phenomena. Trans Tech Publications Ltd, 2010, 160: 63-68.
- [27] Bachmann F, Hielscher R, Schaeben H. Grain detection from 2d and 3d EBSD data--specification of the MTEX algorithm. Ultramicroscopy, 2011, 111(12):1720-1733.
- [28] Germain L, Gey N, Humbert M. Reliability of reconstructed  $\beta$ -orientation maps in titanium alloys. Ultramicroscopy, 2007, 107(2): 1129-1135.
- [29] Zhao Z B, Wang Q J, Hu Q M, et al. Effect of  $\beta$  (110) texture intensity on  $\alpha$ -variant selection and microstructure morphology during  $\beta \rightarrow \alpha$  phase transformation in near  $\alpha$  titanium alloy. Acta Materialia, 2016, 105: 449-463. 2017, 126: 372-382.
- [30] Xavier B, Dorick B D, Julie M, et al. Interfacial characteristics and cohesion mechanisms of linear friction welded dissimilar titanium alloys: Ti-5Al-2Sn-2Zr-4Mo-4Cr (Ti17) and Ti-6Al-2Sn-4Zr-2Mo (Ti6242). Materials Characterization, 2019, 158: 109942.
- [31] Li P, Wang S, Dong H G, et al. Effect of inhomogeneous microstructure evolution on the mechanical properties and corrosion behavior of rotary friction welded AA2024 joints. Materials Characterization, 2021, 178: 111306.
- [32] Jeong W, Yasuhiro A, Kohsaku U, et al. Effect of the welding parameters on microstructure and mechanical properties of linear friction welded Ti-6Al-4V alloy. Journal of Manufacturing Processes, 2022, 75: 651-663.

[33]Jeong W, Yasuhiro A, Kohsaku U, et al. Linear friction welding of Ti-6Al-4V alloy fabricated below  $\beta$ -phase transformation temperature. Scripta Materialia, 2021, 191: 12-16.

[34]Turner R, Gebelin JC, Ward RM, et al. Linear friction welding of Ti-6Al-4V: Modelling and validation. Acta Materialia. 2011, 59(10): 3792-3803.